THE JOURNAL OF PHYSICAL CHEMISTRY LETTERS
A JOURNAL OF THE AMERICAN CHEMICAL SOCIETY

pubs.acs.org/JPCL

Letter

Magneto-Raman Study of Magnon−Phonon Coupling in Two-Dimensional Ising Antiferromagnetic $FePS_3$

Yu-Jia Sun, Jia-Min Lai, Si-Min Pang, Xue-Lu Liu, Ping-Heng Tan, and Jun Zhang*

Cite This: *J. Phys. Chem. Lett.* 2022, 13, 1533−1539

Read Online

ACCESS | Metrics & More | Article Recommendations | Supporting Information

ABSTRACT: Recently, the coupling between magnons (quanta of spin waves) and phonons (quanta of lattice vibrations) in two-dimensional (2D) antiferromagnet $FePS_3$ offers a myriad of applications ranging from spintronic devices to quantum information technologies. However, the reported magnon−phonon coupling in the $FePS_3$ flake using Raman measurements requires an ultrahigh magnetic field up to 30 T. Here, we investigate the magnon−phonon coupling in $FePS_3$ by near-resonant magneto-Raman spectroscopy under a relatively small magnetic field ($|H_0| \leq 9$ T). Under near-resonant excitation, we find more pronounced coupling effects that are absent in non-resonant excitation: three optical phonons sensitive to the applied magnetic field are resolved, two of which show a frequency anti-crossing coupling with magnon, while the other coupled phonon exhibits only a polarization-coupled character without frequency anti-crossing. Besides, our polarized Raman results also show the polarization transferring between coupled magnon−phonon modes. On the basis of a modified theoretical model, we can well explain the measured Raman spectra.

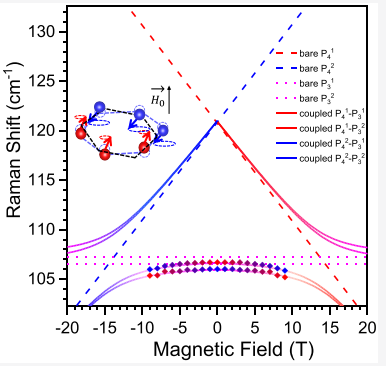

Magnon is a collective excitation of the spins with long-range magnetic order in the magnetic materials.[1] As a result of the absence of a charge current, magnon transport possesses extremely low energy consumption. Therefore, magnonics has rapidly emerged as a novel technology, which exploits the magnon transport to carry and process high-frequency information on the nanoscale.[2] The coupling between spin wave and lattice vibration (magnon−phonon coupling) not only plays a crucial role in the dissipation of energy from the magnon system but also is responsible for many interesting phenomena, including the spin Seebeck effect driven by the local non-equilibrium between phonons and magnons,[3,4] Cherenkov radiation of phonons by magnons,[5] magnon−phonon Kasuya−LeCraw processes,[6] and angular momentum transferring between magnons and phonons.[7]

In addition, new hybrid quasiparticles formed by the coupling of magnons and phonons[8] are of great significance to quantum information and quantum computing applications.[9] Previous studies mainly focus on the ferromagnetic (FM) magnons with intrinsic resonant frequencies in the gigahertz (GHz) range, where the observation of genuine quantum effects needs liquid helium or even millikelvin temperatures. In this particular temperature range, the energies of coherently excited magnons and phonons are comparable to the thermal energy k_BT. In comparison to the FM magnons, antiferromagnetic (AFM) magnons exhibit intrinsic resonant frequencies in the terahertz (THz) range, which can easily reach the quantum ground state even at room temperature. Moreover, the high-frequency AFM magnons possess a much faster speed of processing information, and the AFM ground state is more stable against external magnetic field perturbations than the FM domains.[8] However, the coupling between AFM magnons and high-frequency phonons has not yet been well understood.

The discovery of atomically ultrathin van der Waals (vdW) magnets brings new and exciting possibilities for exploring two-dimensional (2D) magnetism.[10,11] The properties of magnons in 2D magnetic systems win a new degree of freedom connected with spin. One and two magnons have been observed in several 2D magnets, such as $MnPSe_3$, $NiPS_3$, and CrI_3, which sensitively respond to the applied magnetic field.[12−15] In 2020, the quasi-2D AFM magnon in $FePS_3$ was first reported via magneto-Raman spectroscopy.[16] Subsequently, Liu et al. and Vaclavkova et al. reported the direct observation of hybrid magnon−phonon modes in 2D AFM magnet $FePS_3$ by magnetic field-driven resonance, but a high magnetic field up to 30 T is needed to observe the anti-crossing magnon−phonon coupling signature in the eigen spectrum.[8,17] In hybrid magnon−phonon elementary excitation, the phonon dressed in the magnon cloud is related to the spin of electrons, which could be largely renormalized by resonant excitation as a result of electron−phonon coupling.

Received: January 5, 2022
Accepted: February 3, 2022
Published: February 8, 2022

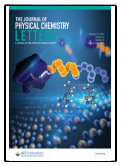

https://doi.org/10.1021/acs.jpclett.2c00023
J. Phys. Chem. Lett. 2022, 13, 1533−1539

Therefore, the resonant excitation could provide a more underlying understanding of magnon−phonon coupling.

Here, we report a Raman spectroscopic study of an AFM $FePS_3$ flake by magnetic field- and polarization-dependent measurements under different excitation energies. We find that the Raman-active mode at 122 cm^{-1} appearing below the Néel temperature T_N (118 K) is an AFM magnon mode. At near-resonant excitation (785 nm), we observe three optical phonons, which are sensitive to the magnetic field. Two of them are coupled to the magnon, forming the magnon−phonon polarons, and the polarization of the other optical phonon depends upon the magnetic field. The frequencies of coupled phonons and magnons deviate significantly from those of the bare magnon and phonons. In contrast to the uncoupled phonons, the magnon and coupled phonons alter their polarization dramatically with the magnetic field. By building the coupled Raman tensor with a linear magnetic dependence, the experimental polarization data can be well reproduced theoretically. Our study opens a possibility for exploring many-body interactions among the magnon, phonon, electron, and photon.

Recently, the strong coupling between the magnon and the phonon has been observed in 2D Ising AFM $FePS_3$, which is of great significance for the development of magnonic devices.[8] Figure 1a shows the lattice structure of bulk $FePS_3$. Iron (Fe)

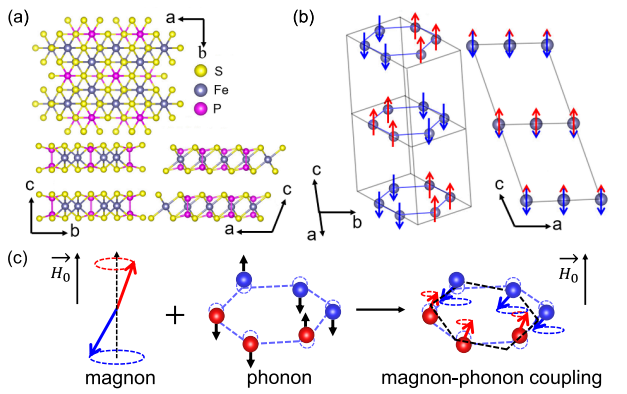

Figure 1. Lattice, spin structures, and coupled magnon−phonon model of $FePS_3$. (a) Schematic structure of the $FePS_3$ crystal, with top and side views of the atomic lattice of the monolayer $FePS_3$ crystal. Gray, pink, and yellow balls represent Fe, P, and S atoms, respectively. (b) AFM structure on the honeycomb lattice of Fe^{2+}. The blue and red arrows represent spin down and spin up, respectively. (c) Microscopic model of the magnon (P_4^1), phonon (P_3), and strong magnon−phonon coupling in $FePS_3$ under an out-of-plane magnetic field H_0. The red (blue) dotted circles represent spin-up (spin-down) precessions. The black arrows represent the vibration directions of Fe^{2+} ions. The blue (black) dotted hexagon corresponds to the lattice structure without (with) the magnetic field.

atoms surrounded by six sulfur (S) atoms and two phosphorus (P) atoms form a honeycomb-like structure in the layer plane,[18] with the interlayer spacing (distance between the center of two adjacent layers) being about 6.42 Å. As shown in Figure 1b, the spin moments of Fe^{2+} ions ($S = 2$) are ordered in the zigzag FM chains as the temperature drops below T_N (118 K), which exhibit both the intra- and interlayer AFM coupling. T_N of $FePS_3$ is almost independent of the layer number.[19] The microscopic model of the magnon−phonon coupling under a high out-of-plane magnetic field, where the frequency of the magnon is in resonance with the phonon, is shown in Figure 1c. When the magnon is coupled to the phonon, the spin of magnon will be transferred to the phonon as a result of the strong magnon−phonon coupling and conservation of momentum.

When the temperature of $FePS_3$ decreases below T_N, the size of the unit cell along the c direction becomes twice as large as that in the paramagnetic phase as a result of the opposite spin directions of consecutive layers in the AFM phase. The renormalized unit cell results in the folding of the Brillouin zone, which activates the non-center phonons.[20] Therefore, four peaks marked as P_1, P_2, P_3, and P_4, respectively, can be observed below T_N. In comparison to the Raman spectra excited by 514 and 633 nm lasers (as shown in Figures S1 and S2 of the Supporting Information), we found that the intensity of P_3 is largely enhanced under near-resonant 785 nm excitation, where the laser energy is close to the bandgap of $FePS_3$ (1.5 eV),[21] as shown in Figure 2a. In addition, a new Raman mode (marked as N) at around 110 cm^{-1} was observed under 785 nm excitation when $|H_0| \geq 2$ T.

As shown in Figure 2a, as the out-of-plane magnetic field increases from 0 to +9 T, the Raman mode P_4 at around 122 cm^{-1} (3.7 THz) splits into two modes (marked as P_4^1 and P_4^2, respectively). The same splitting can be observed with the magnetic field along the $-Z$ direction ranging from 0 to −9 T. The magnetic field-induced splitting further demonstrates that P_4 originates from magnon, which is consistent with previous reports.[16] Magnon is the collective motion in the interacting spin systems with a sequence magnetic (ferromagnetic, ferrimagnetic, or antiferromagnetic) order as a result of various excitations. The frequency of the AFM magnon under a magnetic field is given by[16]

$$\omega_{k=0} = \gamma\{(2H_E + H_A)H_A\}^{1/2} \pm \gamma H_0 \quad (1)$$

where H_E is the exchange field, H_A is the anisotropy field, H_0 is the applied magnetic field, and $\gamma = g\mu_B\mu_0/2\pi\hbar$ is the gyromagnetic ratio. As shown in Figure 2b, according to the linear fitting results using eq 1, the extracted slopes of P_4^1 and P_4^2 branches are −0.99 and +0.99 cm^{-1}/T, respectively, from which we can estimate the effective g factor ($g \approx 2.11$) of the magnon for the $FePS_3$ flake.

In the previous studies, P_3 was reported to manifest a symmetric peak under 488 and 514 nm excitation.[8,16,17,19] In fact, in our high-resolution Raman spectra, P_3 mode shows a tiny asymmetric structure under 514 and 633 nm excitation (Figures S1 and S2 of the Supporting Information), which can be fitted by two Lorentz peaks. However, under the near-resonant excitation (785 nm), these two modes (labeled as P_3^1 and P_3^2) exhibit a more obvious asymmetric line shape, which can only be fitted by two Gaussian peaks (Figure S4 of the Supporting Information). This can be understood as the spectral diffusion induced by electric field fluctuation when the real electronic transition participates,[22] leading to an inhomogeneous broadening of the phonon line shape.[23] The frequencies of P_3^1 and P_3^2 both decrease with the magnetic field ranging from 0 to ±9 T. The frequency difference between P_3^1 and P_3^2 remains a constant as 1.3 ± 0.02 cm^{-1}, indicating that they change synchronously with the magnetic field. In addition, a new mode marked as N mode can be observed under 785 nm excitation. Generally, resonant excitation can active Raman forbidden phonons as a result of strong electron−phonon coupling.[23,24]

According to eq 1, the frequencies of split magnons should vary linearly with the magnetic field. However, as shown in

https://doi.org/10.1021/acs.jpclett.2c00023
J. Phys. Chem. Lett. 2022, 13, 1533−1539

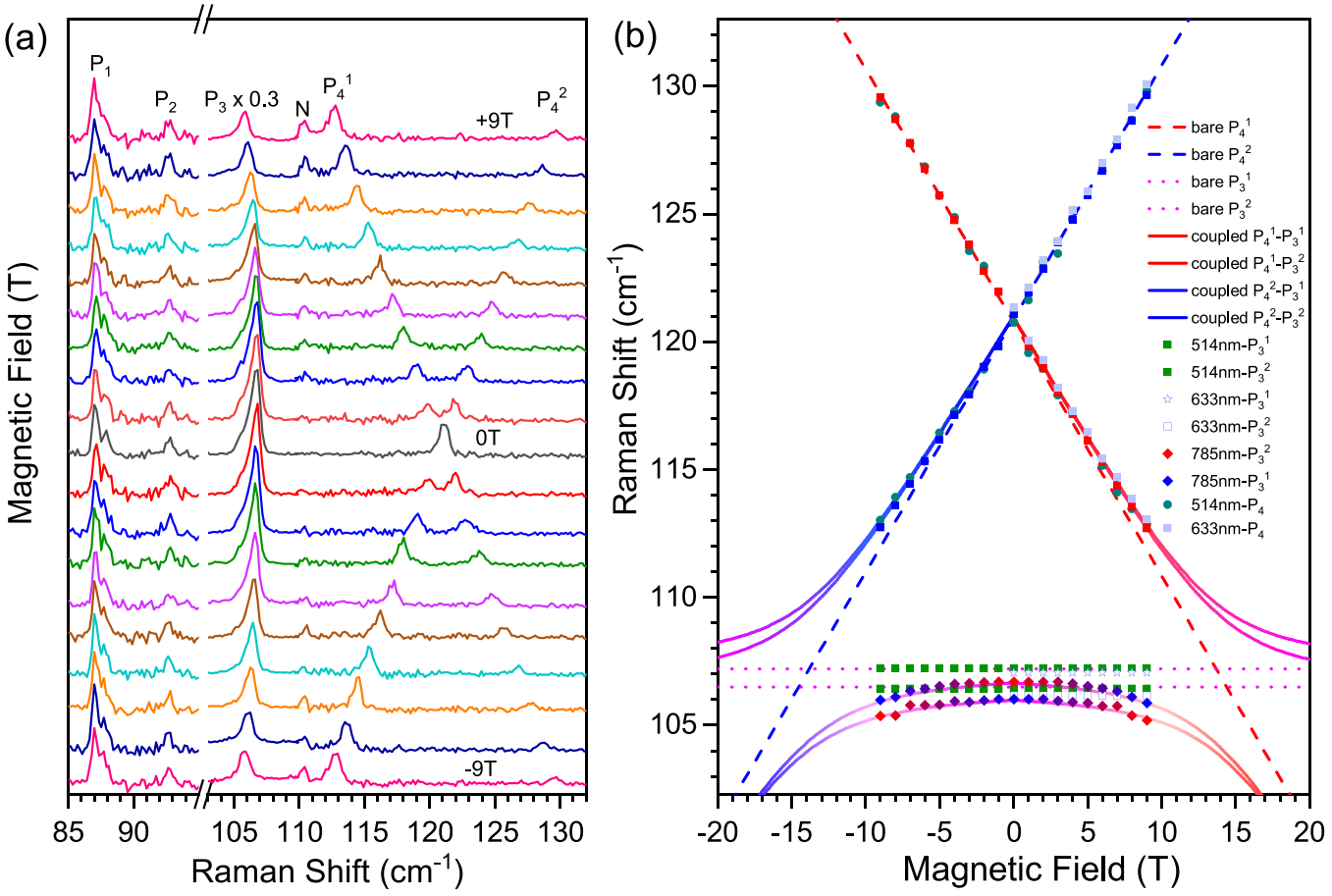

Figure 2. Magnetic field dependence of magnon and phonon modes of the $FePS_3$ flake. (a) Magnetic field-dependent Raman spectra (below 132 cm^{-1}) of $FePS_3$ at 4 K under 785 nm excitation. The intensity of P_3 mode is reduced to 0.3 times the original data. (b) Strong magnon−phonon coupling driven by a magnetic field. The dotted lines represent the frequencies of bare phonon and magnon modes. The solid lines represent the fitting results of the magnon−phonon coupling. Experimental data are denoted by scatter points.

Figure 2b, our high-resolution Raman spectra under 785 nm excitation show that the frequency of P_4^1 deviates from the predicted linear frequency (red dotted line) under the magnetic field along the $+Z$ direction, while the same phenomenon can be observed for P_4^2 under the magnetic field along the $-Z$ direction (blue dotted line). Considering the frequencies of P_3^1 and P_3^2, they decrease with the small magnetic field ranging from 0 to ±9 T under 785 nm excitation while remaining unchanged under 514 nm (green square scatter points) and 633 nm (white square scatter points) excitation. These experimental results illustrate that the low-frequency magnon would interact with the P_3 phonon, and its frequency thus would deviate from the linear frequency of the bare magnon under the 785 nm excitation. Meanwhile, P_3 features an obvious asymmetry and frequency shift under the influence of the magnon. In comparison to the magnon−phonon coupling in the $FePS_3$ flake recently reported through the Raman measurements under the ultrahigh magnetic field up to 30 T,[8,17] here, we can successfully observe the magnon−phonon coupling under a relatively low magnetic field (9 T) by near-resonant Raman spectroscopy. Because the magnon is the precession of the electron spin, the magnon would be affected by conduction electrons through the spin−orbit interaction and electron−phonon scattering.[25,26] The resonance excitation would excite additional electrons and change the electron−phonon coupling, which renormalizes the coupling between the magnon and phonon. Therefore, the magnon−phonon coupling can be observed here at a small magnetic field under near-resonant excitation. The energy dispersion when the magnon (P_4) and phonon (P_3^1 and P_3^2) are strongly coupled is given by[8]

$$\omega^{\pm} = \frac{\omega_M + \omega_{ph}}{2} \pm \frac{1}{2}[(\omega_M - \omega_{ph})^2 + 4|M_c|^2]^{1/2} \quad (2)$$

where ω^+ and ω^- describe the energy dispersion of the two anti-crossing bands induced by the strong coupling between magnons and phonons, ω_M and ω_{ph} are the frequencies of magnons and phonons, respectively, and M_c is the coupling parameter. Under the magnetic field along the $\pm Z$ direction, the P_3 phonon, which vibrates perpendicular to the $a-b$ plane is coupled to the low-frequency magnon, as schematically shown in Figure 1c. Specifically, the magnon coupled to the P_3 phonon under the magnetic field along the $+Z$ direction is P_4^1, while that under the magnetic field along $-Z$ direction is P_4^2. Using eq 2, the theoretical frequency of the strong magnon−phonon coupling mode as a function of the magnetic field is displayed in Figure 2b, which agrees well with our experimental data. According to our fitting results, the frequencies of bare phonons P_3^1 and P_3^2 can be determined as 106.5 and 107.2 cm^{-1}, respectively. Meanwhile, we can obtain the frequencies of bare magnons P_4^1 and P_4^2, which depend upon the magnetic field (H_0) as $121 \pm 0.99H_0$ (T)

https://doi.org/10.1021/acs.jpclett.2c00023
J. Phys. Chem. Lett. 2022, 13, 1533−1539

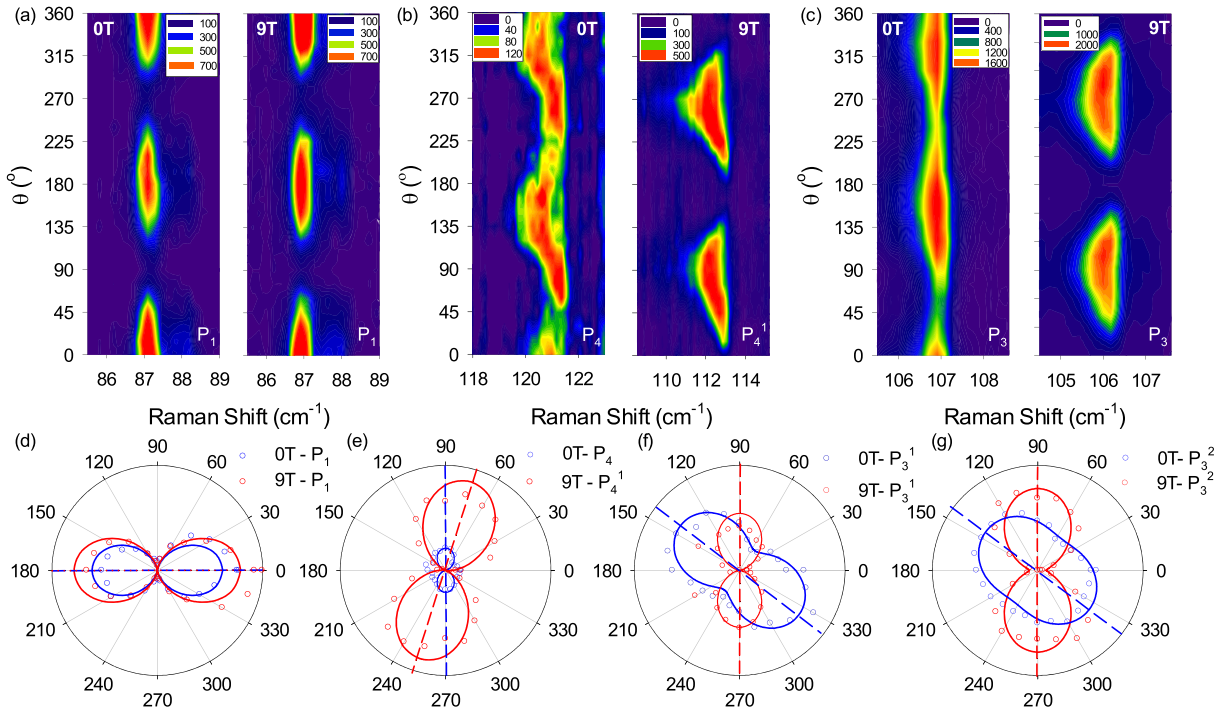

Figure 3. Polarization-dependent Raman spectra of P_1, P_4, P_3^1, and P_3^2. (a) Intensity contour plot of P_1 under 0 and 9 T with θ ranging from 0° to 360°. θ is the angle between the polarization directions of incident and scattered light when the polarization direction of scattered light is fixed. Purple to red colors indicate the intensity variations from zero to maximum. (b) Intensity contour plot of P_4 under 0 T and that of P_4^1 under 9 T. (c) Intensity contour plot of P_3 under 0 and 9 T. Polar graphs of the intensity of (d) P_1, (e) P_4^1, (f) P_3^1, and (g) P_3^2 as a function of the polarization angle θ. The hollow circles represent the experimental data, and the solid curves are the corresponding fitting results. The dotted lines denote the polarization angle θ where the strongest Raman signal appears.

cm^{-1}, and the magnitude of the coupling strength $|M_c|$ is around 2.74 cm^{-1} (82.1 GHz), being consistent with a recent report.[8] Under 514 and 633 nm excitation, the frequencies and line shape of P_3^1 and P_3^2 are independent of the magnetic field. By comparing our experimental data to the theoretical results, we found that the frequencies of bare phonons are very close to those of P_3^1 and P_3^2 under the 514 nm excitation (green square scatter points). As the excitation wavelength increases to 633 nm, the frequencies of P_3^1 and P_3^2 slightly decrease compared to the results under the 514 nm excitation but are still independent of the magnetic field (white square scatter points). Nevertheless, the frequencies of P_3^1 and P_3^2 excited using a 785 nm laser show a significant red shift with the increasing magnitude of the magnetic field, even though the magnetic field is smaller than the reported critical magnetic field (10 T).[8] In comparison to P_3^1 and P_3^2, the frequency of the N mode does not shift with the magnetic field, but its intensity change shows the same magnetic field-dependent trend as the low-frequency magnon. This feature hints that the N mode should be an in-plane vibration mode, whose vibration direction is perpendicular to that of the magnon; therefore, the interaction with the magnon changes its polarization rather than its frequency. The magnetic field impaction on the frequency of P_3 and the intensity of the N mode indicate the interaction among the magnon, electron, and phonon, which still requires further investigations.

In Figure 3a, the intensity and frequency of uncoupled phonon P_1 both exhibit a period of 180° with θ and are independent of the magnetic field. The intensity of P_4^1 under 9 T shows a more obvious period of 180° compared to the intensity of P_4 under 0 T, as shown in Figure 3b. However, the weakest intensity of P_4 under 0 T and that of P_4^1 under 9 T appear at different angles θ. Moreover, the line width and line shape of P_4^1 also change significantly with the magnetic field. P_4^1 can be well-fitted with the Lorentzian line shape at 0°, whereas a single Lorentzian function cannot fit the spectral profile at 90°. Unlike the uncoupled phonon P_1, the polarization behavior of phonon P_3 is more similar to that of the magnon P_4, as shown in Figure 3c. Additionally, the similar behavior of their frequency and line shape varying with the magnetic field further verifies the magnon−phonon coupling in $FePS_3$.

As shown in panels d−g of Figure 3, we plotted the polar graphs of the intensity of P_1, P_4, P_3^1, and P_3^2 as a function of the polarization angle of the incident light under 0 and 9 T. The polar graph of the uncoupled phonon P_1 is independent of the magnetic field, while that of the magnon P_4 and coupled phonon P_3 rotate 20° and 50°, respectively, when the magnetic field alters from 0 to 9 T. The polarization-dependent Raman spectra of uncoupled P_2 and P_4^2 under 0 and 9 T were also measured, as shown in Figure S6b of the Supporting Information. In our backscattering configuration, the polarization directions of both the incident ($\mathbf{e}_i$) and scattered light ($\mathbf{e}_s$) are in the x−y plane, with $\mathbf{e}_i = (\cos\theta, \sin\theta)$ and $\mathbf{e}_s = (1, 0)$, where θ is the angle between $\mathbf{e}_s$ and $\mathbf{e}_i$. The intensity of the scattering signal is related to the Raman tensors of the involved modes: $I \propto |\mathbf{e}_s \cdot \mathbf{R} \cdot \mathbf{e}_i|^2$. In comparison to the polar graphs of P_4 and P_3 under 0 T, those rotate a specific degree under +9 T, which indicates that the magnetic field would modulate their Raman tensors. This can be understood if we revise the Raman tensor with an applied magnetic field H_0 as[27]

$$R = R_{H_0=0} + H_0 R_H \quad (3)$$

https://doi.org/10.1021/acs.jpclett.2c00023
J. Phys. Chem. Lett. 2022, 13, 1533−1539

where $R_{H_0=0}$ is the Raman tensor with $H_0 = 0$ T and R_H is the spin-dependent term. All of the experimental polarization-dependent Raman intensity data can be well-fitted by $I \propto |\mathbf{e}_s \cdot \mathbf{R} \cdot \mathbf{e}_i|^2$, and the fitting results are presented as the solid curves in panels d–g of Figure 3. The bulk $FePS_3$ crystal belongs to the $C2/m$ symmetry group,[28] with 30 irreducible zone center phonon modes denoted by $\Gamma = 8A_g + 6A_u + 7B_g + 9B_u$, where A_g and B_g are Raman active modes. According to the polarized Raman spectra at 0 T, P_1 and P_2 can be assigned as A_g modes. In the backscattering configuration, only 2×2 matrix elements of the Raman tensors can be detected. The Raman tensors of P_1 and P_2 can be described as $A_g = \begin{pmatrix} a & 0 \\ 0 & a \end{pmatrix}$. With the applied magnetic field H_0, the Raman tensor A_g can be rewritten as $R_{A_g} = \begin{pmatrix} a & 0 \\ 0 & a \end{pmatrix} + H_0 \begin{pmatrix} a_- & b_- \\ c_- & d_- \end{pmatrix}$. Because the polarization planes of P_1 and P_2 do not rotate with the magnetic field, we can conclude that R_H for P_1 and P_2 should be symmetric with the form $R_H = \begin{pmatrix} a_- & 0 \\ 0 & d_- \end{pmatrix}$.

According to the theory raised by Fleury and London,[29] the magnon excitations in the magnetic ions with $L = 0$ ground state are purely antisymmetric with the polarization of $\mathbf{e}_s$ and $\mathbf{e}_i$. In Figure 3, P_3 and P_4 can be observed when θ varies from 0° to 360°, which indicates that the symmetry of magnons deviates strongly from the above theory[29] and the Raman tensors of the coupled magnon and phonon are more complicated.[16] In Figure 3e, we can find that the polarization characteristic of P_4 without a magnetic field is similar to that of the B_g mode, whose Raman tensor merely contains the non-zero off-diagonal elements. However, the presence of P_4 at 0° demonstrates that its Raman tensor possesses non-zero diagonal elements. Through fitting with eq 3, we found that the possible Raman tensors of two P_4 peaks are the combination of the forms of A_g and B_g modes.

$$R_{(P_4),A_g} = \begin{pmatrix} 1 & 0 \\ 0 & 1 \end{pmatrix} + H_0 \begin{pmatrix} 1 & 3 \\ 3 & 1 \end{pmatrix}$$

$$R_{(P_4),B_g} = \begin{pmatrix} 0 & 2 \\ 2 & 0 \end{pmatrix} + H_0 \begin{pmatrix} 1 & 3 \\ 3 & 1 \end{pmatrix}$$

In comparison to the polar graph of P_4, those of P_3^1 and P_3^2 rotate 50° counterclockwise under 0 T and their polarization anisotropy is weaker, as shown in panels f and g of Figure 3. The results suggest that their Raman tensors are probably not the combination of the A_g and B_g Raman tensors but include the contribution of the E_g Raman tensor, in which all of the matrix elements are not zero. Through fitting with eq 3, we proposed that the possible Raman tensors for P_3^1 and P_3^2 are a combination of A_g and E_g Raman tensors. The Raman tensors of P_3^1 and P_3^2 can be determined as follows:

$$R_{(P_3^1),A_g} = \begin{pmatrix} -2 & 0 \\ 0 & 2 \end{pmatrix} + H_0 \begin{pmatrix} 0.15 & 0.15 \\ 0.15 & 0.15 \end{pmatrix}$$

$$R_{(P_3^1),E_g} = \begin{pmatrix} -1 & 2 \\ 2 & 1 \end{pmatrix} + H_0 \begin{pmatrix} 0.15 & 0.15 \\ 0.15 & 0.15 \end{pmatrix}$$

$$R_{(P_3^2),A_g} = \begin{pmatrix} 4 & 0 \\ 0 & -4 \end{pmatrix} + H_0 \begin{pmatrix} 0.25 & 0.7 \\ 0.7 & 0.25 \end{pmatrix}$$

$$R_{(P_3^2),E_g} = \begin{pmatrix} -1 & 4 \\ 4 & 1 \end{pmatrix} + H_0 \begin{pmatrix} 0.25 & 0.7 \\ 0.7 & 0.25 \end{pmatrix}$$

It is worth noting that the polar graphs of the coupled phonon P_3 and magnon P_4 can also be reproduced through other linear combinations of the related Raman tensors, but the form of the Raman tensor should be consistent with the above analysis. In summary, according to the magnetic field-dependent polarization Raman spectra, we demonstrate that the polarization behaviors of the coupled magnon–phonon are significantly different from those of the uncoupled modes.

In conclusion, we investigate the properties of hybridized magnon–phonon quasiparticles in the AFM $FePS_3$ flake by magneto-Raman spectroscopy. Under the near-resonant excitation, the coupling between the phonon and magnon is more pronounced than that under the non-resonant excitation. Especially, we have found new phenomena: (1) we can resolve the fine structures of phonon P_3 and find that both submodes of P_3 can couple to magnon to form hybridized magnon–phonon states. (2) A new phonon mode "N" is observed, whose frequency does not alter with the magnetic field, but its polarization depends upon the magnetic field, which indicates that another polarization-coupled mechanism between the magnon and phonon besides frequency anti-crossing possibly exists. Moreover, we propose a possible Raman tensor form of the coupled magnon and phonon under the magnetic field, which can well explain the experimental data. Our results show that the coupling between the magnon and phonon in 2D AFM $FePS_3$ is rather sensitive under the resonant excitation, which hints that the electron–phonon coupling could contribute significantly to the magnon–phonon coupling. Such a many-body system, which includes different elementary excitations, like the phonons, magnons, electrons, and photons, provides an attractive platform to study the emerging many-body quantum effects for further researchers.

■ ASSOCIATED CONTENT

Supporting Information

The Supporting Information is available free of charge at https://pubs.acs.org/doi/10.1021/acs.jpclett.2c00023.

Magnetic field-dependent Raman spectra of $FePS_3$ under the 514, 633, and 785 nm lasers excitation at 4 K, additional experimental details, Gaussian fitting of P_3 mode, and the AFM magnon model under the magnetic field (PDF)

■ AUTHOR INFORMATION

Corresponding Author

Jun Zhang – *State Key Laboratory of Superlattices and Microstructures, Institute of Semiconductors, Chinese Academy of Sciences, Beijing 100083, People's Republic of China; Center of Materials Science and Optoelectronics Engineering and CAS Center of Excellence in Topological Quantum Computation, University of Chinese Academy of Sciences, Beijing 100049, People's Republic of China;* orcid.org/0000-0002-9831-6796; Email: zhangjwill@semi.ac.cn

Authors

Yu-Jia Sun – *State Key Laboratory of Superlattices and Microstructures, Institute of Semiconductors, Chinese Academy of Sciences, Beijing 100083, People's Republic of China; Center of Materials Science and Optoelectronics*

https://doi.org/10.1021/acs.jpclett.2c00023
J. Phys. Chem. Lett. 2022, 13, 1533–1539

Engineering, University of Chinese Academy of Sciences, Beijing 100049, People's Republic of China

Jia-Min Lai − *State Key Laboratory of Superlattices and Microstructures, Institute of Semiconductors, Chinese Academy of Sciences, Beijing 100083, People's Republic of China; Center of Materials Science and Optoelectronics Engineering, University of Chinese Academy of Sciences, Beijing 100049, People's Republic of China*

Si-Min Pang − *State Key Laboratory of Superlattices and Microstructures, Institute of Semiconductors, Chinese Academy of Sciences, Beijing 100083, People's Republic of China; Center of Materials Science and Optoelectronics Engineering, University of Chinese Academy of Sciences, Beijing 100049, People's Republic of China*

Xue-Lu Liu − *State Key Laboratory of Superlattices and Microstructures, Institute of Semiconductors, Chinese Academy of Sciences, Beijing 100083, People's Republic of China*

Ping-Heng Tan − *State Key Laboratory of Superlattices and Microstructures, Institute of Semiconductors, Chinese Academy of Sciences, Beijing 100083, People's Republic of China; Center of Materials Science and Optoelectronics Engineering, University of Chinese Academy of Sciences, Beijing 100049, People's Republic of China;* orcid.org/0000-0001-6575-1516

Complete contact information is available at: https://pubs.acs.org/10.1021/acs.jpclett.2c00023

Notes

The authors declare no competing financial interest.

■ ACKNOWLEDGMENTS

Jun Zhang acknowledges the National Key Research and Development Program of China (Grant 2017YFA0303401), the CAS Interdisciplinary Innovation Team, the National Natural Science Foundation of China (Grant 12074371), and the Strategic Priority Research Program of Chinese Academy of Sciences (Grant XDB28000000).

■ REFERENCES

(1) Costa, A. T.; Santos, D. L. R.; Peres, N. M. R.; Fernández-Rossier, J. Topological magnons in CrI_3 monolayers: an itinerant fermion description. *2D Mater.* **2020**, *7*, 045031.

(2) Bhoi, B.; Kim, S. K. Roadmap for photon-magnon coupling and its applications. *Solid State Phys.* **2020**, *71*, 39−71.

(3) Agrawal, M.; Vasyuchka, V. I.; Serga, A. A.; Karenowska, A. D.; Melkov, G. A.; Hillebrands, B. Direct measurement of magnon temperature: new insight into magnon−phonon coupling in magnetic insulators. *Phys. Rev. Lett.* **2013**, *111*, 107204.

(4) Kubacka, T.; Johnson, J. A.; Hoffmann, M. C.; Vicario, C.; de Jong, S.; Beaud, P.; Grubel, S.; Huang, S. W.; Huber, L.; Patthey, L.; Chuang, Y. D.; Turner, J. J.; Dakovski, G. L.; Lee, W. S.; Minitti, M. P.; Schlotter, W.; Moore, R. G.; Hauri, C. P.; Koohpayeh, S. M.; Scagnoli, V.; Ingold, G.; Johnson, S. L.; Staub, U. Large-amplitude spin dynamics driven by a THz pulse in resonance with an electromagnon. *Science* **2014**, *343*, 1333.

(5) Rückriegel, A.; Kopietz, P.; Bozhko, D. A.; Serga, A. A.; Hillebrands, B. Magnetoelastic modes and lifetime of magnons in thin yttrium iron garnet films. *Phys. Rev. B* **2014**, *89*, 184413.

(6) Kasuya, T.; LeCraw, R. C. Relaxation Mechanisms in Ferromagnetic Resonance. *Phys. Rev. Lett.* **1961**, *6*, 223−225.

(7) Holanda, J.; Maior, D. S.; Azevedo, A.; Rezende, S. M. Detecting the phonon spin in magnon−phonon conversion experiments. *Nat. Phys.* **2018**, *14*, 500−506.

(8) Liu, S.; Granados Del Aguila, A.; Bhowmick, D.; Gan, C. K.; Thu Ha Do, T.; Prosnikov, M. A.; Sedmidubsky, D.; Sofer, Z.; Christianen, P. C. M.; Sengupta, P.; Xiong, Q. H. Direct Observation of Magnon−Phonon Strong Coupling in Two-Dimensional Antiferromagnet at High Magnetic Fields. *Phys. Rev. Lett.* **2021**, *127*, 097401.

(9) Park, S.; Nagaosa, N.; Yang, B. J. Thermal Hall Effect, Spin Nernst Effect, and Spin Density Induced by a Thermal Gradient in Collinear Ferrimagnets from Magnon−Phonon Interaction. *Nano Lett.* **2020**, *20*, 2741−2746.

(10) Ahn, E. C. 2D materials for spintronic devices. *npj 2D Mater. Appl.* **2020**, *4*, 17.

(11) Rivera, N.; Kaminer, I. Light−matter interactions with photonic quasiparticles. *Nat. Rev. Phys.* **2020**, *2*, 538−561.

(12) Wildes, A. R.; Simonet, V.; Ressouche, E.; McIntyre, G. J.; Avdeev, M.; Suard, E.; Kimber, S. A. J.; Lançon, D.; Pepe, G.; Moubaraki, B.; Hicks, T. J. Magnetic structure of the quasi-two-dimensional antiferromagnet $NiPS_3$. *Phys. Rev. B* **2015**, *92*, 224408.

(13) Kim, K.; Lim, S. Y.; Lee, J.-U.; Lee, S.; Kim, T. Y.; Park, K.; Jeon, G. S.; Park, C.-H.; Park, J.-G.; Cheong, H. Suppression of magnetic ordering in XXZ-type antiferromagnetic monolayer $NiPS_3$. *Nat. Commun.* **2019**, *10*, 345.

(14) Gibertini, M.; Koperski, M.; Morpurgo, A. F.; Novoselov, K. S. Magnetic 2D materials and heterostructures. *Nat. Nanotechnol.* **2019**, *14*, 408−419.

(15) Cenker, J.; Huang, B.; Suri, N.; Thijssen, P.; Miller, A.; Song, T.; Taniguchi, T.; Watanabe, K.; McGuire, M. A.; Xiao, D.; Xu, X. D. Direct observation of two-dimensional magnons in atomically thin CrI_3. *Nat. Phys.* **2021**, *17*, 20−25.

(16) McCreary, A.; Simpson, J. R.; Mai, T. T.; McMichael, R. D.; Douglas, J. E.; Butch, N.; Dennis, C.; Valdés Aguilar, R.; Hight Walker, A. R. Quasi-two-dimensional magnon identification in antiferromagnetic $FePS_3$ via magneto-Raman spectroscopy. *Phys. Rev. B* **2020**, *101*, 064416.

(17) Vaclavkova, D.; Palit, M.; Wyzula, J.; Ghosh, S.; Delhomme, A.; Maity, S.; Kapuscinski, P.; Ghosh, A.; Veis, M.; Grzeszczyk, M.; Faugeras, C.; Orlita, M.; Datta, S.; Potemski, M. Magnon polarons in the van der Waals antiferromagnet $FePS_3$. *Phys. Rev. B* **2021**, *104*, 134437.

(18) Tian, Y.; Gray, M. J.; Ji, H. W.; Cava, R. J.; Burch, K. S. Magneto-elastic coupling in a potential ferromagnetic 2D atomic crystal. *2D Mater.* **2016**, *3*, 025035.

(19) Lee, J. U.; Lee, S.; Ryoo, J. H.; Kang, S.; Kim, T. Y.; Kim, P.; Park, C. H.; Park, J. G.; Cheong, H. Ising-Type Magnetic Ordering in Atomically Thin $FePS_3$. *Nano Lett.* **2016**, *16*, 7433−7438.

(20) Hangyo, M.; Nakashima, S.; Mitsuishi, A.; Kurosawa, K.; Saito, S. Raman Spectra of $MnPS_3$ Intercalated with Pyridine. *Solid State Commun.* **1988**, *65*, 419−423.

(21) Du, K. Z.; Wang, X. Z.; Liu, Y.; Hu, P.; Utama, M. I.; Gan, C. K.; Xiong, Q.; Kloc, C. Weak van der Waals Stacking, Wide-Range Band Gap, and Raman Study on Ultrathin Layers of Metal Phosphorus Trichalcogenides. *ACS Nano* **2016**, *10*, 1738−1743.

(22) Wolters, J.; Sadzak, N.; Schell, A. W.; Schroder, T.; Benson, O. Measurement of the ultrafast spectral diffusion of the optical transition of nitrogen vacancy centers in nano-size diamond using correlation interferometry. *Phys. Rev. Lett.* **2013**, *110*, 027401.

(23) Tan, Q. H.; Sun, Y. J.; Liu, X. L.; Xu, K. X.; Gao, Y. F.; Ren, S. L.; Tan, P. H.; Zhang, J. Breakdown of Raman selection rules by Fröhlich interaction in few-layer WS_2. *Nano Res.* **2021**, *14*, 239−244.

(24) Tan, Q. H.; Sun, Y. J.; Liu, X. L.; Zhao, Y. Y.; Xiong, Q. H.; Tan, P. H.; Zhang, J. Observation of forbidden phonons, Fano resonance and dark excitons by resonance Raman scattering in few-layer WS_2. *2D Mater.* **2017**, *4*, 031007.

(25) Kamberský, V. Spin-orbital Gilbert damping in common magnetic metals. *Phys. Rev. B* **2007**, *76*, 134416.

(26) Lai, J. M.; Xie, Y. R.; Zhang, J. Detection of electron-phonon coupling in two-dimensional materials by light scattering. *Nano Res.* **2021**, *14*, 1711−1733.

(27) McCreary, A.; Mai, T. T.; Utermohlen, F. G.; Simpson, J. R.; Garrity, K. F.; Feng, X.; Shcherbakov, D.; Zhu, Y.; Hu, J.; Weber, D.;

Watanabe, K.; Taniguchi, T.; Goldberger, J. E.; Mao, Z.; Lau, C. N.; Lu, Y.; Trivedi, N.; Valdés Aguilar, R.; Hight Walker, A. R. Distinct magneto-Raman signatures of spin-flip phase transitions in CrI_3. *Nat. Commun.* **2020**, *11*, 3879.

(28) Wang, X. Z.; Du, K. Z.; Liu, Y. Y. F.; Hu, P.; Zhang, J.; Zhang, Q.; Owen, M. H. S.; Lu, X.; Gan, C. K.; Sengupta, P.; Kloc, C.; Xiong, Q. H. Raman spectroscopy of atomically thin two-dimensional magnetic iron phosphorus trisulfide ($FePS_3$) crystals. *2D Mater.* **2016**, *3*, 031009.

(29) Fleury, P. A.; Loudon, R. Scattering of Light by One- and Two-Magnon Excitations. *Phys. Rev.* **1968**, *166*, 514−530.

https://doi.org/10.1021/acs.jpclett.2c00023
J. Phys. Chem. Lett. 2022, 13, 1533−1539